Editors' Suggestion | Featured in Physics

Spectroscopy of Quantum Dot Orbitals with In-Plane Magnetic Fields

Leon C. Camenzind,[1] Liuqi Yu,[1] Peter Stano,[2,3,4] Jeramy D. Zimmerman,[5,†] Arthur C. Gossard,[5] Daniel Loss,[1,2] and Dominik M. Zumbühl[1,*]

[1]*Department of Physics, University of Basel, Klingelbergstrasse 82, CH-4056 Basel, Switzerland*
[2]*Center for Emergent Matter Science, RIKEN, Saitama 351-0198, Japan*
[3]*Department of Applied Physics, School of Engineering, University of Tokyo, 7-3-1 Hongo, Bunkyo-ku, Tokyo 113-8656, Japan*
[4]*Institute of Physics, Slovak Academy of Sciences, 845 11 Bratislava, Slovakia*
[5]*Materials Department, University of California, Santa Barbara, California 93106, USA*

(Received 31 March 2018; revised manuscript received 5 February 2019; published 22 May 2019)

We show that in-plane magnetic-field-assisted spectroscopy allows extraction of the in-plane orientation and full 3D size parameters of the quantum mechanical orbitals of a single electron GaAs lateral quantum dot with subnanometer precision. The method is based on measuring the orbital energies in a magnetic field with various strengths and orientations in the plane of the 2D electron gas. From such data, we deduce the microscopic confinement potential landscape and quantify the degree by which it differs from a harmonic oscillator potential. The spectroscopy is used to validate shape manipulation with gate voltages, agreeing with expectations from the gate layout. Our measurements demonstrate a versatile tool for quantum dots with one dominant axis of strong confinement.

DOI: 10.1103/PhysRevLett.122.207701

A spin in a magnetic field is one of the simplest canonical quantum two-level systems encoding a qubit [1]. To realize spin-based quantum computing, the capability of addressing individual spin qubits is essential, as demonstrated in various semiconductor quantum dot devices [2]. Although significant progress has been made on the control of spin states, the challenge lies in the lack of means to adjust the confinement potential, particularly for dot systems formed in nanowires or by intrinsic defects. Lateral quantum dots, on the other hand, show excellent flexibility. Defined in a 2D electron gas (2DEG) by nanometer-scale surface gates, they allow, in principle, arbitrary and tunable dot shapes [3].

This tunability is important for spin manipulations. Namely, the dot shape and the related orbital energy spectrum are directly associated with a variety of spin-electric related processes. These rely on mixing of spin and orbital degrees of freedom since the orbital shape determines the dipole moments connected with spin-flip transitions. For instance, such mixing presents the predominant channel for spin relaxation in GaAs, through both the spin-orbit [3–5] and hyperfine interactions [6,7]. Both spin relaxation [3] and spin manipulation by electric-dipole spin resonance (EDSR) [8,9] show a strong dependence on the dot shape and the orientation in the 2DEG plane and with respect to the magnetic field. The dependence can be exploited to control both the spin relaxation time and EDSR frequency [10].

The bottleneck in taking full advantage of this flexibility is that, so far, there is no direct method to adequately determine the quantum dot confinement geometry. Many previous experiments probed low-lying excited-state energies [3,6,11,12]. However, there are characteristics of the confinement that are difficult to disentangle from such measurements (the potential anharmonicity), which are energetically not accessible (the subband spacing) and which are not present in such data at all (the dot orientation).

Looking for alternative ways to extract these characteristics is full of obstacles, too: since the dot is imprinted into the 2DEG beneath the surface of the device, details of the dot shape are inaccessible for surface imaging tools, such as atomic force or scanning tunneling microscopy. Also, the electric fields from the surface gates will in return interfere with the probe aggravating such measurements [13,14]. Further, these methods suffer from invasive backaction of the probe to the sample disturbing the quantum dot. In principle, nowadays, software is capable of advanced simulations [11,15]. However, the reliable input to such simulations is restricted to the design of the surface gates and the chemical composition used during the wafer growth. The details of the interfaces, strain distribution, and, most importantly, impurities and donor positions are unknown. At the moment, they can be at best guessed and included into such simulations by hand. Formation of unintentional dots, and dots with positions and shapes differing from the one suggested by the gate layout, is more a rule than an exception. Finally, the fact that the dot details often change upon cooldown is proof that, even though simulations can serve as a rough guide, they are unable to provide sample-dependent details.

In this Letter, we present a noninvasive technique that is able to extract the 3D shape and orientation parameters of

the quantum mechanical orbitals of a quantum dot with subnanometer precision. It is based on a response of the energy spectrum to an in-plane magnetic field of varying magnitude and direction. The theoretical principles of the method are explained in Ref. [16]. Here, we demonstrate it experimentally. While our quantitative interpretation of the measurements is based on assuming an asymmetric (triangular) 2DEG confinement and a harmonic in-plane confinement, the method is directly applicable to any quasi-two-dimensional system for which the unperturbed confinement can be reasonably guessed.

The surface gate layout of the measured device, shown in Fig. 1(a), is based on Ref. [3]. The device is biased into the single-electron quantum dot regime, as indicated by the red ellipsoid. The dot is tuned to couple to the left reservoir only, with a tunnel rate between 1 and 100 Hz. An additional quantum dot, located directly adjacent to the main dot, serves as a charge sensor [22,23], giving a change of sensor conductance of up to 100% per electron in the main dot. The sample can be oriented with an essentially arbitrary angle with respect to an in-plane magnetic field up to 14 T using a piezoelectric rotator. Using standard van der Pauw measurements, the magnetic field is shown to deviate less than 1.3° out of the 2DEG plane, thus rendering the out-of-plane component negligible [6]. Measurements are done in a dilution refrigerator with an electron temperature of 60 mK [24–26].

The orbital energies are measured by pulsed-gate spectroscopy using a three-step pulse sequence. Namely, an additional voltage ΔV_P is applied to the center plunger gate (CP), on top of the static gate voltage V_P [see Fig. 1(a)] [3,27,28]. As illustrated in Fig. 1(b), the sequence consists of initialization, charging, and readout steps (see also Sec. V in the Supplemental Material [17]). The elastic tunnel rate into the empty dot increases sharply when an orbital state becomes resonant with the chemical potential μ of the reservoir. By measuring the dot-reservoir tunnel coupling for varying ΔV_P, individual excited orbital states can be distinguished. An example is shown in Fig. 1(c) exhibiting three excited orbital states. The ground state, which calibrates $\Delta V_P = 0$, couples much weaker to the reservoir ($\Gamma_{GS} \sim 10$ Hz) compared to the excited orbital states, attributed to the increased spatial extent of higher orbitals [29,30]. The exponential decay in the tunnel rate of the excited states with increasing ΔV_P [dashed curves in Fig. 1(c)] is due to an increasing tunnel barrier [31–33]. Finally, we note that our method requires that the probe voltage does not change the confinement potential. We conclude that this assumption is well met, as the pulse ΔV_P is much smaller (typically, tens of millivolts, applied only on one gate) than voltages required to change the dot shape substantially (typically hundreds of millivolts, applied on all gates), as deduced from Fig. 2(a).

We assume that the dot confinement separates into a 2D harmonic oscillator part for the in-plane coordinates and a much stronger confinement for the heterostructure growth direction ($\hat{z}$) coordinate,

$$H = \frac{\mathbf{p}^2}{2m} + \frac{\hbar^2}{2m}\left(\frac{x_d^2}{l_x^4} + \frac{y_d^2}{l_y^4}\right) + v(z). \quad (1)$$

Here, $\mathbf{p}$ is the momentum operator, $\hbar$ is the reduced Planck constant, m is the effective mass, and $l_{x,y}$ are the confinement lengths along the main axes $\hat{x}_d$ and $\hat{y}_d$ of the in-plane confinement. These axes are, in general, rotated from the crystal axes [100] and [010] by an angle δ [see Figs. 1(a)

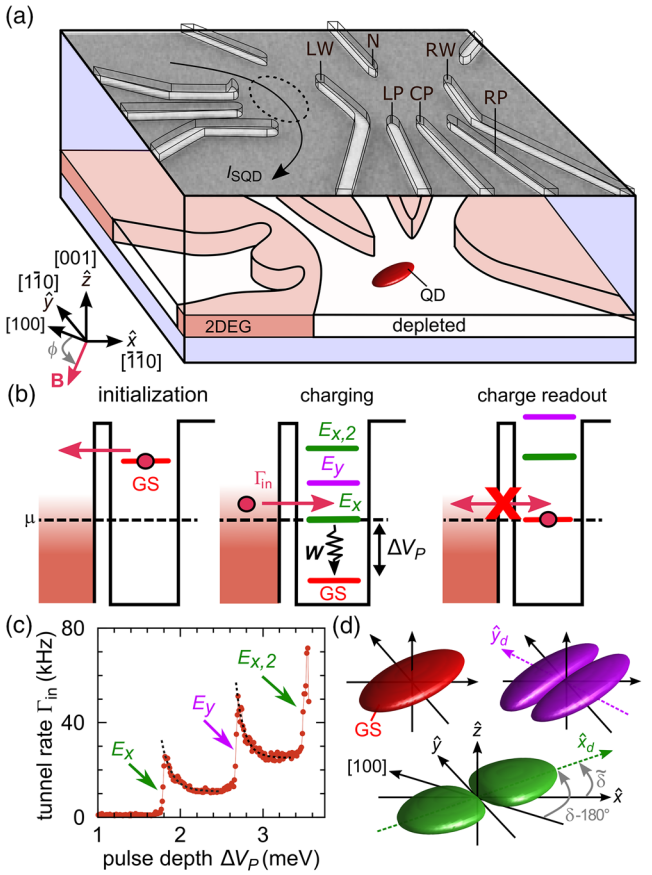

FIG. 1. (a) Sketch with electron micrograph of the gate layout of a cofabricated device shown on top. The gate left wall (LW), right wall (RW), left plunger (LP), center plunger (CP), right plunger (RP) and nose (N) form the quantum dot (QD). The sensor quantum dot (SQD) is adjacent to the left. The $GaAs/Al_{0.3}Ga_{0.7}As$ heterostructure contains a 2DEG with density 2.6×10^{11} cm^{-2} and mobility 4×10^5 cm^2/V s located 110 nm below the surface. The in-plane field angle ϕ and wave function orientation δ are defined with respect to [100], while $\tilde{\delta} = \delta - 225°$ is the angle between $\hat{x} = [\bar{1}\,\bar{1}\,0]$ and $\hat{x}_d$, the dot confinement x axis. (b) Three-step pulse sequence described in the text. (c) Measurement of tunneling-in rate Γ_{in} as a function of ΔV_P exhibiting three excited orbital states at energies E_x, E_y, and $E_{x,2}$. (d) Ground-state wave function (left) and the p-type orbitals for an elongated dot with exaggerated anisotropy (details in Sec. I of the Supplemental Material [17]).

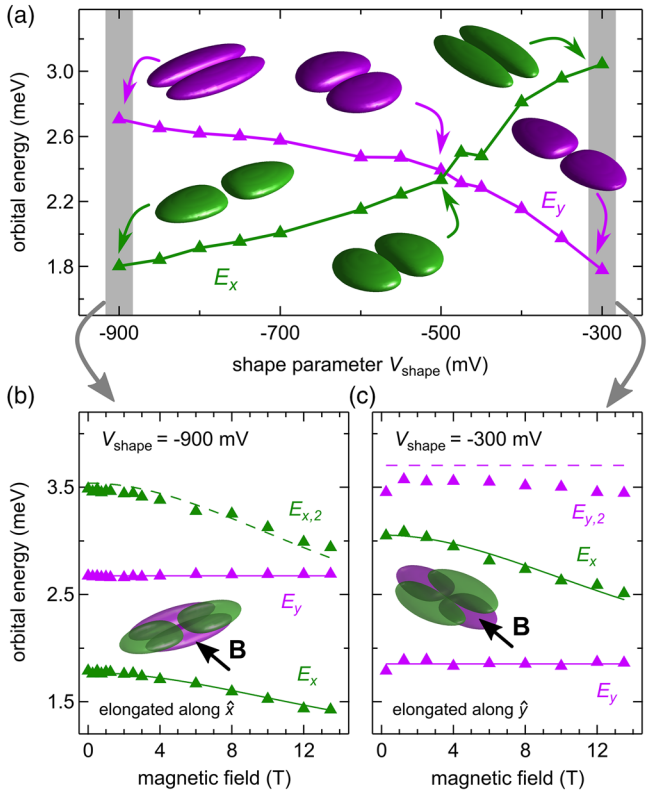

FIG. 2. (a) Orbital excitation energies E_x (green) and E_y (purple) as a function of V_{shape}. The schematics give a qualitative picture of the excited orbital wave functions along the $\hat{x}$ direction (green) and $\hat{y}$ direction (purple) for the three shapes indicated by the arrows. Less exaggerated wave functions are shown in Sec. I of the Supplemental Material [17]. Orbital excitation energies for a magnetic field applied along the y direction for two extreme dot shapes elongated (b) along $\hat{x}$ and (c) along $\hat{y}$, for V_{shape} as labeled. The data are fitted to Eq. (4), giving $\lambda_z = 6.3 \pm 0.3$ nm and $E_z = 28.6 \pm 3$ meV [34].

and 1(d)]. For simplicity, we introduce $\tilde{\delta} = \delta - 225°$ as the angle between potential axis $\hat{x}_d$ and device axis $\hat{x} = [\bar{1}\,\bar{1}\,0]$. In the model described by Eq. (1), the excitation energies are $E_{x,y} = \hbar^2/ml_{x,y}^2$ and the ground-state wave function can be represented by a disklike ellipsoid. The two lowest excited states correspond to p-like orbitals aligned along two perpendicular axes $\hat{x}_d$, $\hat{y}_d$, as shown in Fig. 1(d).

Within this model, the parameters E_x, E_y, and δ characterize the dot shape, and vice versa, control of these parameters indicates dot-shape tunability. This is what we demonstrate next. Applying appropriate voltages on the surface gates, the dot can be elongated either in the $\hat{x}$ or, alternatively, the $\hat{y}$ direction [3]. For instance, the dot can be squeezed in the $\hat{y}$ direction by applying more negative voltages on the plunger gates LP, CP, and RP [see Fig. 1(a)]. To keep the ground-state energy constant, these changes are compensated by applying less negative voltages on the other gates LW and RW, which leads to an expansion of the wave function in the $\hat{x}$ direction. We introduce a shape parameter V_{shape} to denote the full set of gate voltages corresponding to a particular configuration (see Fig. 2), with the numerical value of V_{shape} taken to be the voltage on gate CP.

The two lowest orbital excitation energies are shown in Fig. 2(a) as a function of the dot shape V_{shape}. Upon making V_{shape} more negative, thus squeezing the dot in the $\hat{y}$ direction, one of the two energies increases, thus identified as the $\hat{y}$ state. The other energy decreases and thus has to be the $\hat{x}$ state, as labeled in Fig. 2. Interestingly, at $V_{\text{shape}} \sim -500$ mV, we find $E_x \approx E_y$, indicating a circular, isotropic wave function in the 2D plane. Such shape manipulation by gate voltages is limited, on one hand, by the minimum voltage needed to deplete the 2DEG underneath the surface gates and, on the other hand, by the gate leakage threshold at more negative gate voltages. We emphasize that, throughout the shape manipulation, the tunneling rate to the reservoir is held approximately constant. For each dot shape, the relevant lever arm is measured, providing the gate voltage to energy conversion in order to obtain the excited-state energies from pulsed-gate spectroscopy (see Sec. IV in the Supplemental Material [17] for details).

From such data, however, there is no estimate of the tilt angle $\tilde{\delta}$ or how it depends on V_{shape}—other than that it is probably not too big. It is natural to expect that, as the dot is being squeezed, the wave function is also shifted and possibly somewhat rotated in space, depending on the detailed potential and disorder landscape present. In addition, we note that the subband excitations $E_z \gg E_{x,y}$ are energetically out of reach of this pulsed-gate spectroscopy method, so that little can be said about the size of the dot orbitals along the growth axis. We are now going to show how this missing information can be revealed; this is the main advance that our work makes.

To this end, we exploit the effects of a strong in-plane magnetic field $\mathbf{B}$ applied along an in-plane direction $\hat{b}$, which makes an angle ϕ with the [100] crystallographic axis [see coordinate system in Fig. 1(a)]. In Ref. [16], we show that the leading order effect can be expressed as a correction to Eq. (1) of the following form [35]:

$$\delta H = -\frac{\Phi^2}{2m}[\mathbf{p} \cdot (\hat{b} \times \hat{z})]^2. \tag{2}$$

This interaction is the basis for our spectroscopy. Its strength scales with the magnetic flux Φ penetrating the 2DEG due to its finite width. Explicitly,

$$\Phi = \frac{e}{\hbar} B \lambda_z^2, \tag{3}$$

where $e > 0$ is the elementary charge and λ_z is the effective width of the wave function along the growth direction. We analyze the connection between a nominal width and the effective width of a 2DEG for several confinement profiles, namely, triangular, harmonic, and a square potential

well [16]. Also, we note that flux threading was previously studied in open dots [36–38].

For typical 2DEGs and magnetic fields, the flux is small: $\Phi \ll 1$ [34]. Treating Eq. (2) as a perturbation to Eq. (1), the energies change by

$$\delta E_{x,y} = -\frac{\Phi^2}{2}\frac{\hbar^2}{m l_{x,y}^2}\sin^2(\delta_{x,y} - \phi). \tag{4}$$

Here, we denoted $\delta_{x,y}$ as the corresponding excited orbital directions (with respect to [100]). They follow from Eq. (1) as $\delta_x = \delta$ and $\delta_y = \delta + \pi/2$.

First, we apply a strong magnetic field along the y direction for the two most elongated shapes available [see Figs. 2(b) and 2(c)]. For sufficiently weak confinement along one direction, a second excited state $E_{x,2}$ or $E_{y,2}$ also becomes accessible. While $E_{x,2} \sim 2E_x$ for the dot in Fig. 2(b), $E_{y,2}$ is slightly lower in energy than the second harmonic of E_y, as seen in Fig. 2(c). For this configuration, the voltage on the nose N and all plunger gates are only barely sufficient to deplete the 2DEG, which could lead to a softening of the confinement potential along $\hat{y}$. Looking at the field dependence, we make the striking observation that E_y remains constant for both shapes, while E_x clearly changes with magnetic field. This is consistent with the notion that the orbital effects of a magnetic field are given by a Lorentz force, which is a vector product of the velocity with the field, thus leaving motion along the direction of the applied field unaffected. This agrees with the prediction of Eq. (2), giving that $\hat{x}_d \approx \hat{x}$, meaning that the dot is oriented along the device axes. The invariance of E_y indicates that the corresponding orbital is rather well aligned with the magnetic field and therefore the y axis of the device. Comparing the two cases in Fig. 2, we emphasize that, going from Fig. 2(b) to 2(c), the quantum dot was in fact rotated by 90°, thus demonstrating a gate-induced quantum dot *rotation*. Indeed, this is expected from the gate voltage dependence V_{shape} and is here validated in real space with the in-plane field spectroscopy.

By fitting the data to Eqs. (3) and (4), we can extract the effective width λ_z and thus the size of the quantum dot along the growth direction. We can convert the latter, under a rather mild assumption that the heterostructure confinement is triangular, to the interface electric field E_{ext} and the subband energy splitting E_z. This in turn allows for the evaluation of the spin-orbit fields. Namely, from $\lambda_z = 6.3 \pm 0.3$ nm, we get the spin-orbit lengths $l_r = 2.1 \pm 0.3$ μm and $l_d = 3.2 \pm 0.3$ μm for the Rashba and Dresselhaus interaction, respectively [39]. Using an independent fit from the directional variation of the spin-relaxation time [6] gave $l_r = 2.5 \pm 0.2$ μm and $l_d = 4.1 \pm 0.4$ μm illustrating the agreement. We point out that, apart from determining the spin-orbit interactions strengths, the width of the 2DEG determines also the strength the electron Fermi contact interaction with nuclear spins. Thus, knowledge on the quantum dot size along the growth direction is essential for quantitative analysis of spin properties, such as relaxation [6].

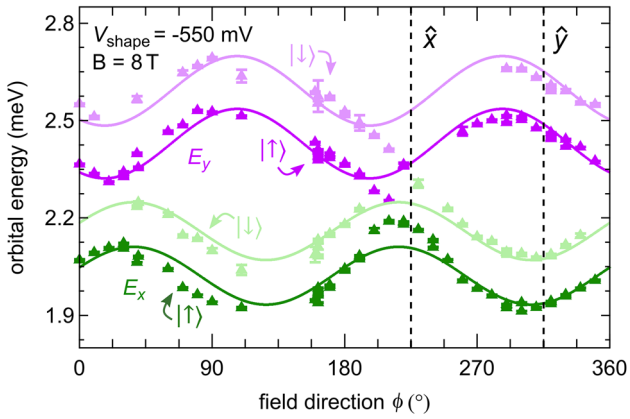

FIG. 3. Spin-resolved excitation energies measured at the magnetic field of a fixed magnitude 8 T and varying direction in an almost circular quantum dot ($V_{\text{shape}} \sim -550$ mV in Fig. 2). The solid curves show a fit according to Eq. (4) for each orbital state (separately for the green and purple data) assuming a direction-independent Zeeman energy. Since the g factor anisotropy is small [40], this is a very good approximation. The fit gives $\tilde{\delta}_x = -8° \pm 4°$, $\tilde{\delta}_y = 62° \pm 4°$, and $\lambda_z = 6.1 \pm 0.3$ nm ($E_z = 30.7 \pm 3$ meV) [34].

We now turn to a precise quantification of the dot orientation. It can be done by measuring the excitation energies at a magnetic field with fixed magnitude and varied orientation. Figure 3 presents such data for $B = 8$ T and a more symmetric dot. The energies show a sinusoidal behavior as expected from Eq. (4). The two states oscillate out of phase, proving that they represent orbitals oriented perpendicular to each other (see also Sec. III in the Supplemental Material [17]). For an elongated (quasi-1D) dot, the states would oscillate in phase [16]. Beyond confirming that our dot is indeed close to a symmetric one, we can specify its orientation in detail. By fitting the data of Fig. 3 to Eqs. (1) and (2), we obtain $\tilde{\delta} = -8° \pm 4°$, indicating the dot is slightly tilted away from the device coordinate system. We note that even such modest misalignment can have a large impact on the qubit quality [10] and on characterization of the spin-orbit fields [4].

Before concluding, we look at the assumption that the in-plane confinement is a quadratic function of coordinates, adopted in Eq. (1). It has been used from the onset of quantum dot investigations [11] as a practical choice for which analytical solutions are known [41–43]. Compared to its prevalent use, the evidence on such confinement shape is less abundant and has, until now, been restricted to checking the equidistant energy spacing of excited states of a harmonic oscillator. The data in Fig. 3 can provide additional information. Namely, fitting each of the accessible orbitals to Eq. (4) *individually*, we can extract the x, y orbital-specific angle $\delta_{x,y}$. In principle, one can map out the

dependence of δ on the single-particle state energy, if more excited states are accessible. Here, we find $\delta_y - \delta_x \approx 70 \pm 8°$. It is different from 90°, a value for a purely quadratic potential, and here we have quantified by how much.

In summary, we measure excitation energies in a single-electron lateral quantum dot with in-plane magnetic fields of varying orientation. We show that such measurement can determine the orientation of the dot and extract its single-particle quantum mechanical confinement parameters. In particular, this means that, for a given orbital, one can assign a size and orientation within the 2DEG plane, as well as its extension along the growth direction with subnanometer resolution. The information on the quantum dot shape has an immediate use in correct quantification of the spin-orbit fields, as well as the strength of the electron-nuclear Fermi contact hyperfine interaction. We note that the method is directly applicable to any quasi-2D dot, also in other materials and more sophisticated structures, for example, triple quantum dot devices with noncollinear arrangement, as well as dots with higher electron occupations, where Hartree-Fock orbitals could be accessed in the same way.

The data that support the findings of this study are available in a Zenodo repository [44].

We thank V. Golovach for valuable inputs and stimulating discussions, M. Steinacher and S. Martin for technical support, and Basel Precision Instruments GmbH for specialized electronics, such as preamplifiers and voltage sources. This work was supported by the Swiss Nanoscience Institute (SNI), NCCR QSIT, Swiss NSF, ERC starting grant (DMZ), and the European Microkelvin Platform (EMP). P. S. acknowledges support from CREST JST (JPMJCR1675) and JSPS Kakenhi Grant No. 16K05411.National Center of Competence in Research Quantum Science and Technology

*Corresponding author.
dominik.zumbuhl@unibas.ch
†Present address: Physics Department, Colorado School of Mines, Golden, Colorado 80401, USA.

[1] D. Loss and D. P. DiVincenzo, Phys. Rev. A **57**, 120 (1998).
[2] C. Kloeffel and D. Loss, Annu. Rev. Condens. Matter Phys. **4**, 51 (2013).
[3] S. Amasha, K. MacLean, I. P. Radu, D. M. Zumbühl, M. A. Kastner, M. P. Hanson, and A. C. Gossard, Phys. Rev. Lett. **100**, 046803 (2008).
[4] P. Scarlino, E. Kawakami, P. Stano, M. Shafiei, C. Reichl, W. Wegscheider, and L. M. K. Vandersypen, Phys. Rev. Lett. **113**, 256802 (2014).
[5] V. N. Golovach, A. Khaetskii, and D. Loss, Phys. Rev. Lett. **93**, 016601 (2004).
[6] L. C. Camenzind, L. Yu, P. Stano, J. D. Zimmerman, A. C. Gossard, D. Loss, and D. M. Zumbühl, Nat. Commun. **9**, 3454 (2018).
[7] S. I. Erlingsson and Y. V. Nazarov, Phys. Rev. B **66**, 155327 (2002).
[8] K. C. Nowack, F. H. L. Koppens, Y. V. Nazarov, and L. M. K. Vandersypen, Science **318**, 1430 (2007).
[9] M. Pioro-Ladrière, T. Obata, Y. Tokura, Y.-S. Shin, T. Kubo, K. Yoshida, T. Taniyama, and S. Tarucha, Nat. Phys. **4**, 776 (2008).
[10] O. Malkoc, P. Stano, and D. Loss, Phys. Rev. B **93**, 235413 (2016).
[11] S. M. Reimann and M. Manninen, Rev. Mod. Phys. **74**, 1283 (2002).
[12] R. Hanson, L. P. Kouwenhoven, J. R. Petta, S. Tarucha, and L. M. K. Vandersypen, Rev. Mod. Phys. **79**, 1217 (2007).
[13] M. A. Topinka, B. J. LeRoy, R. M. Westervelt, S. E. J. Shaw, R. Fleischmann, E. J. Heller, K. D. Maranowski, and A. C. Gossard, Nature (London) **410**, 183 (2001).
[14] A. Pioda, S. Kičin, T. Ihn, M. Sigrist, A. Fuhrer, K. Ensslin, A. Weichselbaum, S. E. Ulloa, M. Reinwald, and W. Wegscheider, Phys. Rev. Lett. **93**, 216801 (2004).
[15] M. Stopa, Phys. Rev. B **54**, 13767 (1996).
[16] P. Stano, C.-H. Hsu, L. C. Camenzind, L. Yu, D. M. Zumbühl, and D. Loss, Phys. Rev. B **99**, 085308 (2019).
[17] See Supplemental Material at http://link.aps.org/supplemental/10.1103/PhysRevLett.122.207701 for wave functions, in-plane B-field energy corrections, orbital spectra, lever arms, and measurement details, including Refs. [18–21].
[18] S. Gustavsson, R. Leturcq, B. Simovič, R. Schleser, P. Studerus, T. Ihn, K. Ensslin, D. C. Driscoll, and A. C. Gossard, Phys. Rev. B **74**, 195305 (2006).
[19] L. Casparis, M. Meschke, D. Maradan, A. C. Clark, C. P. Scheller, K. K. Schwarzwälder, J. P. Pekola, and D. M. Zumbühl, Rev. Sci. Instrum. **83**, 083903 (2012).
[20] S. D. Liles, R. Li, C. H. Yang, F. E. Hudson, M. Veldhorst, A. S. Dzurak, and A. R. Hamilton, Nat. Commun. **9**, 3255 (2018).
[21] P. Stano and J. Fabian, Phys. Rev. B **77**, 045310 (2008).
[22] M. Field, C. G. Smith, M. Pepper, D. A. Ritchie, J. E. F. Frost, G. A. C. Jones, and D. G. Hasko, Phys. Rev. Lett. **70**, 1311 (1993).
[23] C. Barthel, M. Kjargaard, J. Medford, M. Stopa, C. M. Marcus, M. P. Hanson, and A. C. Gossard, Phys. Rev. B **81**, 161308(R) (2010).
[24] C. P. Scheller, S. Heizmann, K. Bedner, D. Giss, M. Meschke, D. M. Zumbühl, J. D. Zimmerman, and A. C. Gossard, Appl. Phys. Lett. **104**, 211106 (2014).
[25] D. Maradan, L. Casparis, T.-M. Liu, D. E. F. Biesinger, C. P. Scheller, D. M. Zumbühl, J. D. Zimmerman, and A. C. Gossard, J. Low Temp. Phys. **175**, 784 (2014).
[26] D. E. F. Biesinger, C. P. Scheller, B. Braunecker, J. Zimmerman, A. C. Gossard, and D. M. Zumbühl, Phys. Rev. Lett. **115**, 106804 (2015).
[27] J. M. Elzerman, R. Hanson, L. H. Willems Van Beveren, L. M. K. Vandersypen, and L. P. Kouwenhoven, Appl. Phys. Lett. **84**, 4617 (2004).
[28] A. C. Johnson, C. M. Marcus, M. P. Hanson, and A. C. Gossard, Phys. Rev. B **71**, 115333 (2005).
[29] T. Fujisawa, Y. Tokura, and Y. Hirayama, Phys. Rev. B **63**, 081304(R) (2001).

[30] R. Hanson, B. Witkamp, L. M. K. Vandersypen, L. H. Willems van Beveren, J. M. Elzerman, and L. P. Kouwenhoven, Phys. Rev. Lett. **91**, 196802 (2003).
[31] K. MacLean, S. Amasha, I. P. Radu, D. M. Zumbühl, M. A. Kastner, M. P. Hanson, and A. C. Gossard, Phys. Rev. Lett. **98**, 036802 (2007).
[32] S. Amasha, K. MacLean, I. P. Radu, D. M. Zumbühl, M. A. Kastner, M. P. Hanson, and A. C. Gossard, Phys. Rev. B **78**, 041306(R) (2008).
[33] P. Stano and P. Jacquod, Phys. Rev. B **82**, 125309 (2010).
[34] A generalization beyond this regime is given in Supplemental Material Sec. 2 and Ref. [16] and boils down to the replacement $\Phi^2 \to 1 - 1/(1+\Phi^2)$ in Eqs. (2) and (4), which was used in fitting the data here, too. A more sophisticated fitting, beyond the perturbative regime, can be done straightforwardly [16], leading to only small changes in the values of extracted parameters.
[35] F. Stern, Phys. Rev. Lett. **21**, 1687 (1968).
[36] V. I. Fal'ko and T. Jungwirth, Phys. Rev. B **65**, 081306(R) (2002).
[37] D. M. Zumbühl, J. B. Miller, C. M. Marcus, V. I. Fal'ko, T. Jungwirth, and J. S. Harris, Phys. Rev. B **69**, 121305(R) (2004).
[38] D. M. Zumbühl, J. B. Miller, C. M. Marcus, D. Goldhaber-Gordon, J. S. Harris, K. Campman, and A. C. Gossard, Phys. Rev. B **72**, 081305(R) (2005).
[39] The error intervals on the spin-orbit lengths given here are due to the uncertainty in λ_z. We do not reflect additional uncertainty, stemming from the conversion factors (basically, uncertainty in parameters of the $k \cdot p$ theory).
[40] P. Stano, C.-H. Hsu, M. Serina, L. C. Camenzind, D. M. Zumbühl, and D. Loss, Phys. Rev. B **98**, 195314 (2018).
[41] B. Schuh, J. Phys. A **18**, 803 (1985).
[42] I. M. Davies, J. Phys. A **18**, 2737 (1985).
[43] T. K. Rebane, Theor. Exp. Chem. **5**, 1 (1972).
[44] L. C. Camenzind, L. Yu, P. Stano, J. D. Zimmerman, A. C. Gossard, D. Loss, D. M. Zumbühl, Supporting data for spectroscopy of quantum dot orbitals with in-plane magnetic fields (2019), https://doi.org/10.5281/zenodo.2652371.